Susceptibility of Polar Flocks to Spatial Anisotropy

Alexandre Solon, Hugues Chaté, John Toner, Julien Tailleur

Susceptibility of Polar Flocks to Spatial Anisotropy

Alexandre Solon,[1] Hugues Chaté,[2,3,1] John Toner,[4] and Julien Tailleur[5]

[1] *Sorbonne Université, CNRS, Laboratoire de Physique Théorique de la Matière Condensée, 75005 Paris, France*
[2] *Service de Physique de l'Etat Condensé, CEA, CNRS Université Paris-Saclay, CEA-Saclay, 91191 Gif-sur-Yvette, France*
[3] *Computational Science Research Center, Beijing 100094, China*
[4] *Department of Physics and Institute for Fundamental Science, University of Oregon, Eugene, OR 97403*
[5] *Université de Paris, Laboratoire Matière et Systèmes Complexes (MSC), UMR 7057 CNRS, 75205 Paris, France*

(Dated: April 5, 2022)

We study the effect of spatial anisotropy on polar flocks by investigating active q-state clock models in 2D. Unlike the equilibrium case, we find that any amount of anisotropy is asymptotically relevant, drastically altering the phenomenology from that of the rotationally-invariant case. All of the well-known physics of the Vicsek model, from giant density fluctuations to micro-phase separation, is replaced by that of the Active Ising model, with short-range correlations and complete phase separation. These changes appear beyond a lengthscale that diverges in the $q \to \infty$ limit so that the Vicsek-model phenomenology is observed in finite systems for weak enough anisotropy, *i.e.* sufficiently high q. We provide a scaling argument which explains why anisotropy has such different effects in the passive and active cases.

Active matter, being made of energy-consuming units, is well known to exhibit spectacular collective behaviors not permitted in equilibrium. Experimental examples include the defect dynamics of active nematics [1–3], low Reynolds number turbulence [4, 5], motility-induced phase separation [6–8] and, perhaps most famously, flocking [9–13]. Although these phenomena appear in complex, usually living, systems, most of our theoretical understanding comes from studying collections of identical active units evolving in pristine environments, often with periodic boundary conditions. Recently acquired evidence suggests, though, that active systems seem to be fundamentally sensitive to quenched and population disorder [14–20], and that even the nature of boundaries can influence bulk properties [21].

The sensitivity of active systems to anisotropy, in the form of fixed preferred directions in space, remains largely unexplored. A basic result is available in the context of polar flocks, *i.e.* collections of simple self-propelled particles locally aligning their velocities. In two space dimensions, comparing the Vicsek model (VM) [22] to the active Ising model (AIM) [23] shows that the symmetry of the order parameter controls the emerging physics. In the VM, dynamics are rotation invariant, i.e., have continuous symmetry, and the ordered phase exhibits scale-free density and order fluctuations [24–28]. In the AIM, directed motion happens only along two opposite directions, hence the dynamics only has a discrete symmetry, and the correlations are short ranged in the ordered phase. Concomitantly, even though the transition to collective motion is akin to a phase-separation scenario in both the AIM and the VM, their coexistence phases are different [29]: models in the Vicsek class exhibit microphase separation, typically in the form of a smectic train of traveling dense bands [30], whereas the AIM shows a single moving domain and macrophase separation [31].

Anisotropy is generically expected in experimental systems, due to weak external fields. The AIM, by restricting directed motion along one dimension, corresponds to an extreme spatial anisotropy, whose relevance for realistic systems can be questioned. A natural question is then whether polar flocks and the physics of the Vicsek model are robust to weaker forms of anisotropy. In equilibrium, the 2D XY model—which is the passive counterpart of the VM—is in a sense both robust and sensitive to the discreteness of spins: q-state clock models, which break rotational invariance and interpolate between the XY and the Ising models, exhibit a quasi-long-range ordered phase similar to that of the XY model below the BKT transition for $q > 4$, but this critical phase gives way to a region of long-range order below some finite temperature that vanishes only when $q \to \infty$ [32–36]. Thus, from the XY viewpoint, a new ordered phase emerges at any q, but it is marginal, confined to $T = 0$, in the $q \to \infty$ limit.

In this Letter, we investigate the susceptibility of polar flocks to weak anisotropy. Using a combination of numerical simulations and analytical arguments, we study q-state active clock models and their hydrodynamic theories. We uncover a scenario qualitatively different from the equilibrium one: the phenomenology of the rotationally invariant Vicsek model disappears for any amount of spin anisotropy, leaving only AIM-like phenomenology with short-ranged correlations and macrophase separation. This, however, happens only asymptotically: at fixed q, one still observes the Vicsek physics up to a typical scale ξ_q that diverges exponentially with q, which we estimate using a mean-field theory and a scaling argument. The latter traces back the fundamental difference with equilibrium to the presence of long-range order in the isotropic active system.

Active clock models. Particles $i = 1, \dots, N$ carrying a spin $s_i \in \{0, 1, \dots, q-1\}$ reside at the nodes $\mathbf{R}$ of

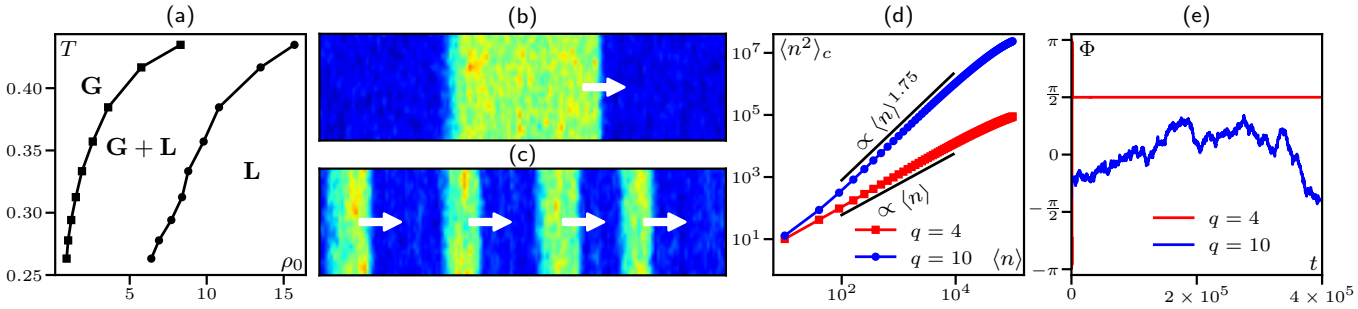

FIG. 1. **(a)** Typical phase diagram in the (ρ_0, T) plane ($q = 4$), Transition lines are defined by the coexisting densities at a given temperature $T = 1/\beta$, computed in systems of size 400×20). **(b,c)**: Snapshots of density field in the coexistence phase in a long 800×20 system suitable for the observation of many traveling bands (steady state, $\rho_0 = 10$, $q = 4$ in (b), $q = 10$ in (c)). **(d)** Number fluctuations $\langle n^2\rangle_c$ vs $\langle n\rangle = \rho_0\ell^2$, the number of particles in a square box of linear size ℓ calculated in the liquid phase of square 200×200 systems ($\rho_0 = 10$, $\beta = 3.5$). "Giant" anomalous fluctuations are observed for $q = 10$, but not for $q = 4$. **(e)** Time series of $\Phi \equiv \arg\langle \mathbf{m}_k\rangle_k$, the orientation of the global polar order (parameters as in (d)).

a square lattice without occupation constraints. They undergo biased diffusion by jumping to neighboring sites with rate $D(1+\varepsilon \mathbf{d}\cdot\mathbf{u}_i)$ with $\mathbf{d}$ the direction of the jump and $\mathbf{u}_i = (\cos\theta_i, \sin\theta_i)$ the unit vector along the clock angle $\theta_i = 2\pi s_i/q$. Spins can rotate to the previous or next "hour" $\theta_i' \equiv \theta_i \pm \frac{2\pi}{q}$ at rate

$$w_{i,\mathbf{R}} = w_0 \exp\left[\frac{\beta}{2\rho_{\mathbf{R}}}\mathbf{m}_{\mathbf{R}}\cdot(\mathbf{u}_i' - \mathbf{u}_i)\right] \qquad (1)$$

where $\rho_{\mathbf{R}}$ and $\mathbf{m}_{\mathbf{R}} = \sum_{j\in\mathbf{R}}\mathbf{u}_j$ are, respectively the number of particles and the magnetization at site $\mathbf{R}$ hosting particle i, $\mathbf{u}_i'$ is the new spin direction, and w_0 is a constant [37]. For $q = 2$, one recovers the AIM used in [31]. As shown in [38], in the isotropic $q \to \infty$ limit, the spin dynamics reduces to the Langevin equation

$$\partial_t\theta_i = \Omega_\infty + \sqrt{2D_\infty}\xi_i \qquad (2)$$

where ξ_i is a Gaussian white noise of unit variance and the torque and rotational diffusivity are given by $\Omega_\infty = \frac{4w_0\pi^2\beta}{q^2}\left(\frac{\mathbf{m}_{\mathbf{R}}}{\rho_{\mathbf{R}}}\cdot\frac{\partial\mathbf{u}_i}{\partial\theta_i}\right) + O(q^{-3})$ and $D_\infty = \frac{4w_0\pi^2}{q^2} + O(q^{-3})$, respectively. In order to have a well-behaved active XY model in the $q \to \infty$ limit, one must thus take $w_0 \propto q^2$. In the following, we set $w_0 = \frac{q^2}{4\pi^2}$ to fix $D_\infty = 1$ and choose $D = 1$ without loss of generality. For simplicity, we also fix the activity parameter $\varepsilon = 0.9$. [39]

The only parameters left to vary, in addition to q, are thus the temperature $T = 1/\beta$ and the global density $\rho_0 = N/(L_xL_y)$, where L_x and L_y define a rectangular domain with periodic boundary conditions. For numerical efficiency, we use parallel updating, first performing on-site spin rotations, then biased jumps.

Phase diagrams in the (ρ_0, T) plane at fixed q all resemble those of the AIM or VM: the disordered gas present at high T and/or low ρ_0 is separated from the low-T/high-ρ_0 polarly-ordered liquid by a coexistence phase (Fig. 1a). The liquid and coexistence phases both have a finite global magnetization $m \equiv |\langle\mathbf{m}_{\mathbf{R}}\rangle_{\mathbf{R}}|$. However, at fixed system size, they display AIM-like or VM-like properties depending on q: For large q, one observes giant number fluctuations in the polar liquid and microphase separation, as for the Vicsek model (Fig. 1c,d). At lower q values, on the contrary, the liquid has normal fluctuations and the system phase separates into a single moving domain (Fig. 1b,d). The direction of global order $\Phi \equiv \arg\langle\mathbf{m}_{\mathbf{R}}\rangle_{\mathbf{R}}$ also behaves differently in the liquid phase, hence distinguishing AIM-like and VM-like behaviors: $\Phi(t)$ wanders slowly at large q, whereas it is pinned along a clock angle at small q (Fig. 1e). The results presented in Fig. 1 seem to suggest that active clock models have different behavior at $q = 4$ and $q = 10$, similar to the differences between the AIM and the VM. In fact this is only true at finite size, as we now show in both the liquid and phase-separated phases.

We first consider the behavior of correlation func-

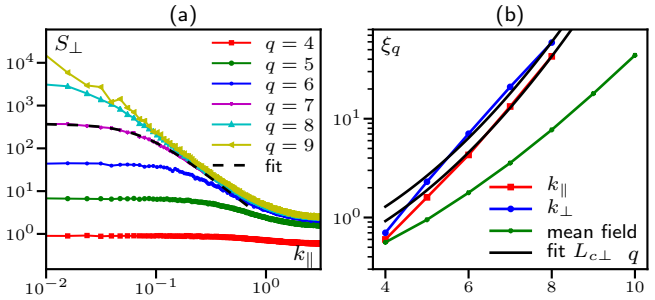

FIG. 2. Liquid phase of active clock models ($\rho_0 = 5.5$, $\beta = 4$, system size 800×800): (a) $S_\perp(\mathbf{k}) = \langle m_\perp(\mathbf{k})m_\perp(-\mathbf{k})\rangle$ vs $\mathbf{k} = (k_\parallel, 0)$ for $q \in [\![4, 9]\!]$. For $q = 7$ we show the fit to the Ornstein-Zernicke function $\alpha/(1 + (\xi k)^2)$, (dashed line). (b) Crossover length ξ_q. For red and blue symbols, ξ_q is obtained by Ornstein-Zernicke fits of $S_\perp(\mathbf{k})$ using $\mathbf{k} = (k_\parallel, 0)$ and $\mathbf{k} = (0, k_\perp)$, respectively. The green curve is the mean-field prediction derived from Eq. (5). The black line corresponds to $L_{c\perp}(q)$, predicted by our scaling argument fitting only the prefactor a in Eq. (9).

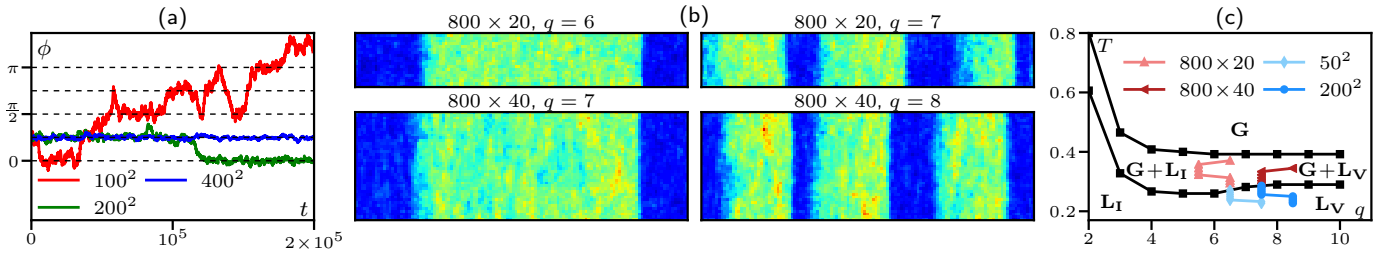

FIG. 3. Transition from the Vicsek to the active Ising behavior as system size increases. **(a)**: Direction of global order in the liquid phase showing a transition between unpinned and pinned as system size increases. The dashed lines indicate the hours of the clock. $\beta = 4$, $\rho_0 = 5.5$, $q = 8$. **(b)**: Snapshots of the density obtained after a long time $t = 5 \times 10^5$ starting from a large ordered band. The transition is shifted to larger q as L increases. Same color code as in Fig. 1. $\beta = 3.2$, $\rho_0 = 5.5$. **(c)**: Phase diagram in the $q - T$ plane at $\rho_0 = 5.5$. The line between macro- $(G + L_I)$ and micro-phase separation $(G + L_V)$ is defined as the transition between a single and multiple bands after time $t = 10^6$ at the system size indicated in the legend. The line separating the two liquids (L_I and L_V) is defined as the transition between pinned and unpinned order parameter orientation after time $t = 10^5$.

tions in the liquid phase. In Fig. 2a, we show the transverse magnetization structure factor $S_\perp(\mathbf{k}) = \langle m_\perp(\mathbf{k}) m_\perp(-\mathbf{k})\rangle$ for wavelength $\mathbf{k}$ calculated in large systems for various q values (the same behavior is observed for the structure factor of the density field). For sufficiently small q, $S_\perp$ converges to finite values as $\mathbf{k} \to 0$. This AIM-like behavior only happens, though, beyond a crossover length scale ξ_q. For scales smaller than ξ_q, the structure factor exhibits algebraic scaling, as in the VM. The crossover scale ξ_q can be extracted by fitting the structure factors to the Ornstein-Zernicke function $f(k) = \alpha/(1 + (\xi_q k)^2)$ [40]. This yields a typical scale ξ_q that increases exponentially rapidly with q (Fig. 2b). Extrapolating these results, we expect that, even for large q values, VM behavior will be observed in the liquid phase up to (large) finite sizes, but that the asymptotic behavior at the largest length scales is Ising-like. Consistently, we observe a transition from unpinned to pinned order parameter in the liquid phase as L increases at fixed q (Fig. 3a).

Importantly, the crossover from VM to AIM phenomenology is also observed in the phase-coexistence region. Systems with linear size $L \ll \xi_q$ exhibit microphase separation, as in the VM. On the contrary, for $L \gg \xi_q$, the systems show full phase separation as in the AIM. Fig. 3b illustrates this: the transition from microphase to macrophase separation happens upon increasing the transverse system size at fixed q, whereas the reverse transition is seen upon increasing q at fixed system size.

The crossover from VM to AIM behavior can be summarized in the (q, T) phase diagram at fixed global density. The three expected phases are present, but one can, at a given system size, define boundaries between Ising and Vicsek behavior within the coexistence and the liquid-phase regions, as shown in Fig. 3c and described in its caption. These boundary lines are displaced to higher and higher q values as the system size is increased. Extrapolating to the infinite-size limit, VM-like behavior is singular, confined to the infinite-q (active XY) limit. Note that the transitions in the coexistence and liquid phases happen at different system sizes in Fig. 3c. We believe this to be due to the peculiar and poorly understood mechanism by which the Vicsek-type long-range correlated fluctuations break the phase separation into a microphase separation [29]. This need not happen at the same system size as the pinning of the order parameter in the liquid although the underlying physics —a cross-over from Ising-like to Vicsek-like physics—is the same.

Effective continuous description. In equilibrium, clock models are sometimes described at the field-theoretical level as continuous spins subjected to an anisotropic potential $V_q(\phi)$ [32], where ϕ parameterizes the local direction of order. While usually postulated on symmetry grounds, we have derived this potential at large q using a mean-field approximation [38], which yields

$$V_q(\phi) = -\frac{2\rho}{\beta}\frac{I_q(\beta|\mathbf{m}|/\rho)}{I_0(\beta|\mathbf{m}|/\rho)}\cos(q\phi) \tag{3}$$

with $\mathbf{m}$ and ρ the local magnetization and density, $\phi = \arg(\mathbf{m})$, and $I_n(x)$ the modified Bessel function of the first kind. Equation (3) is only the leading order contribution at large q, but direct comparisons with simulations of the fully connected clock model show that it is already a good approximation for $q = 4$ [38].

We now demonstrate that we can understand the behavior of our microscopic active clock model using the mean-field hydrodynamic description of its isotropic, $q = \infty$ limit complemented by the anisotropic potential (3). This hydrodynamic theory, derived in [38] with standard techniques akin to those used for the AIM [31], reads

$$\partial_t \rho = D\Delta\rho - v\nabla\cdot\mathbf{m} \tag{4a}$$

$$\partial_t \mathbf{m} = \left(\tfrac{\beta}{2} - 1 - \tfrac{\beta^2}{8\rho^2}\mathbf{m}^2\right)\mathbf{m} + D\Delta\mathbf{m} - \tfrac{\beta}{\rho}\partial_\phi V_q(\phi)\,\mathbf{m}^\perp + \tfrac{\beta v}{4\rho}(\mathbf{m}^\perp\nabla\cdot\mathbf{m}^\perp - \mathbf{m}\nabla\cdot\mathbf{m}) - \tfrac{v}{2}\nabla\rho\,, \tag{4b}$$

where $\mathbf{m}^\perp \equiv (-m_y, m_x)$.

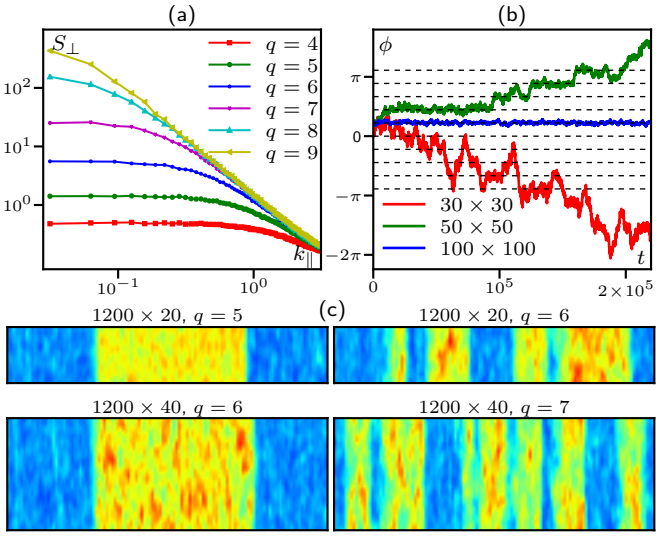

FIG. 4. Simulations of the PDE with noise (a) Structure factor $S_\perp(\mathbf{k}) = \langle m_\perp(\mathbf{k}) m_\perp(-\mathbf{k})\rangle$ vs $\mathbf{k} = (k_\parallel, 0)$ in the ordered phase for several q values (system size 200×200). (b) Time series of the orientation of global order Φ in the ordered phase showing a transition between unpinned and pinned dynamics as the system size increases ($q = 9$). (c) Simulations with the additional density-dependent term necessary to observe band solutions [38]. As in Fig. 3 (b), snapshots of the density after a long time $t = 5 \times 10^5$ starting from a large ordered band. Parameters: $\beta = 4$, $D = 1$, $v = 1.8$, $\rho_0 = 5.5$ (a,b) and $\rho_0 = 1.85$ (c).

Consider a perturbation of the homogeneous ordered state $\mathbf{m} = (m_0 + \delta m_\parallel, \delta m_\perp)$. To linear order, using $\sin q\phi \approx q\phi \approx q m_\perp / m_\parallel$, we obtain for the $m_\perp$ field

$$\dot{\delta m_\perp} = D\Delta \delta m_\perp + \{\text{drift terms}\} - \alpha_q \delta m_\perp \qquad (5)$$

with $\alpha_q = 2q^2 \frac{I_q(\beta m_0/\rho_0)}{I_0(\beta m_0/\rho_0)}$. When $\alpha_q = 0$, there is no mass on $m_\perp$. This happens happens when $q \to \infty$, as expected from the continuous rotational symmetry. With $\alpha_q > 0$ however, a mass damps the fluctuations of $m_\perp$ and therefore pins the direction of order. The typical length scale on which this damping occurs is $\xi = \sqrt{D/\alpha_q}$, which compares well to the crossover length ξ_q measured in the microscopic model (Fig. 2b) albeit—unsurprisingly—not quantitatively. To account for the structure factor reported in Fig. 2 for the microscopic model, we complement Eq. (4b) with an isotropic centered Gaussian white noise field $\boldsymbol{\eta}(\mathbf{r}, t)$ of unit variance. The structure factor of $m_\perp$, shown in Fig. 4a, is found to be qualitatively similar to that of Fig. 2. Moreover a pinning transition occurs when L is increased (Fig. 4b), as in Fig. 3a for the microscopic models.

Our hydrodynamic description also captures the nature of the coexistence region. Complementing Eq. (4b) with the density-dependent coefficients needed to account for inhomogeneous profiles [38], we show in Fig. 4c that increasing q at a given system size leads from macro- to micro-phase separation whereas the converse happens when increasing L at fixed q. Again, the VM phenomenology is observed at large q and small sizes, whereas AIM physics is found to be the asymptotic behaviour at large L.

Scaling argument. All in all, anisotropy is thus always relevant asymptotically. This is markedly different from what happens in equilibrium where, for $q > 4$, there is a range of temperature over which the anisotropy is irrelevant asymptotically, and one observes quasi-long-range order, as for a continuous spin. The argument used to derive a crossover length from the linearized hydrodynamic equation in Eq. (5) therefore fails in equilibrium. Indeed, there is no homogeneous ordered state to perturb from, only a quasi-ordered state with algebraically decaying correlations. This difference is essential, as is clear from looking at the scaling with system size of the energy $H_q = \int d^2\mathbf{r} \cos(q\theta(\mathbf{r}))$ due to the "clock potential".

Let us then compare the scaling with L of $\langle H_q\rangle_0$, where the average is taken in the unperturbed system without H_q, in equilibrium and in the active case. Of course, we do not actually have a Hamiltonian in this last case, but this argument should roughly capture the effect of the potential in the equation of motion (4). In equilibrium, the unperturbed state can be described by the spinwave Hamiltonian $H_0 = \int d^2\mathbf{r} \frac{K}{2} [\nabla\theta(\mathbf{r})]^2$ with stiffness K. The perturbation is then evaluated as

$$\langle H_q\rangle_0 \approx \int d^2\mathbf{r} \langle e^{iq\theta(\mathbf{r})}\rangle_0 = \int d^2\mathbf{r} e^{-\frac{q^2}{2} G(\mathbf{0})} \qquad (6)$$

where G is the Green function of the Laplacian in infinite space. In Fourier space $\hat{G}(\mathbf{k}) = \frac{T}{Kk^2}$, which, in 2D, gives $G(\mathbf{0}) = T\log(L/\Lambda)/(2\pi K)$ for a system of size L, with Λ a short distance cut-off. Inserting this into Eq. (6) yields

$$\langle H_q\rangle_0 \sim L^{2-\frac{q^2 T}{4\pi K}} . \qquad (7)$$

Equation (7) predicts anisotropy to be relevant as $L \to \infty$ whenever $T < T_q \equiv \frac{8\pi K}{q^2}$ and irrelevant otherwise. If $T_q < T_{BKT} \equiv \frac{\pi K}{4}$, which happens for $q > q_c = 4$, one observes a quasi-long range ordered phase where anisotropy is irrelevant for $T_q < T < T_{\mathrm{BKT}}$, and a long-range ordered phase where anisotropy is relevant for $T < T_q$.

In the active case, the ordered state of the unperturbed system is long-range ordered. Assuming that $\theta(\mathbf{r})$ shows Gaussian fluctuations with variance σ^2 around its mean value θ_0 leads to $\langle e^{iq\theta(\mathbf{r})}\rangle_0 = e^{-q^2\sigma^2/2}$. In turn, Eq. (6) becomes

$$\langle H_q\rangle_0^{\text{active}} \approx \int \mathbf{d^2 r} \langle e^{iq\theta(\mathbf{r})}\rangle_0 = L^2 e^{-q^2\sigma^2/2} \qquad (8)$$

Anisotropy is thus always relevant when $L \gg L_q \equiv e^{q^2\sigma^2/4}$, so that $\langle H_q\rangle_0^{\text{active}} \gg 1$. For $L \ll L_q$, on the contrary, anisotropy is exponentially suppressed by q and Vicsek physics may be observed.

The argument above qualitatively explains the different responses to anisotropy observed in the active and passive cases. In equilibrium, it has been made more rigorous using renormalization group calculations [32, 33]. In the active case, its essential conclusions hold within a dynamical renormalization group analysis [24, 27] which shows that the lengthscale $L_{c\perp}$ beyond which the symmetry-breaking field changes the physics obeys [41]

$$L_{c\perp}(q,\sigma) = a \exp\left[q^2\sigma^2/(2z)\right] . \tag{9}$$

where a is a microscopic length and z a dynamic exponent whose most recent numerical estimate is $z \simeq 1.33$ [28]. After measuring σ in a microscopic simulation [42], we show in Fig. 2b that the prediction of Eq. (9) is consistent with the observed crossover length.

Conclusion. We have shown that polar flocks are strongly altered, at large scales, by spatial anisotropy. This is reflected by the suppression of hallmark features of the Vicsek model: in the liquid phase the correlations are short ranged, not scale free, the direction of order is pinned, not wandering; and one has macrophase instead of microphase separation at coexistence. Interestingly, these changes occur only beyond a characteristic lengthscale that diverges for vanishingly small anisotropy and large q. In the liquid and coexistence regions, the crossover from VM to AIM physics can be understood using a hydrodynamic description where anisotropy is accounted for by an effective potential. In the liquid phase, the difference with the passive case can be explained using a scaling argument, which shows that the presence of long-range order is sufficient to render the anisotropy relevant asymptotically for any value of q and T.

Our study calls for understanding spatial anisotropy in other active-matter systems, like active nematics. Finally, the absence of any effect of the anisotropy of the lattice used in our clock model —our results hold for an off-lattice version— is almost surprising. Whether lattice anisotropy couples to the aligning dynamics at larger scales than those considered here surely deserves further study.

We thank Mourtaza Kourbane-Houssene for his early involvement in this work, and Benoît Mahault for a critical reading of the manuscript. This work was partially supported by the French ANR through projects NeqFluids to HC and THEMA to JT.

[1] T. Sanchez, D. T. Chen, S. J. DeCamp, M. Heymann, and Z. Dogic, Nature **491**, 431 (2012).
[2] H. Li, X.-q. Shi, M. Huang, X. Chen, M. Xiao, C. Liu, H. Chaté, and H. Zhang, Proceedings of the National Academy of Sciences **116**, 777 (2019).
[3] G. Duclos, R. Adkins, D. Banerjee, M. S. Peterson, M. Varghese, I. Kolvin, A. Baskaran, R. A. Pelcovits, T. R. Powers, and A. Baskaran, Science **367**, 1120 (2020).
[4] H. H. Wensink, J. Dunkel, S. Heidenreich, K. Drescher, R. E. Goldstein, H. Löwen, and J. M. Yeomans, Proceedings of the National Academy of Sciences **109**, 14308 (2012).
[5] V. A. Martinez, E. Clément, J. Arlt, C. Douarche, A. Dawson, J. Schwarz-Linek, A. K. Creppy, V. Škultéty, A. N. Morozov, and H. Auradou, Proceedings of the National Academy of Sciences **117**, 2326 (2020).
[6] I. Buttinoni, J. Bialké, F. Kümmel, H. Löwen, C. Bechinger, and T. Speck, Physical Review Letters **110**, 238301 (2013).
[7] D. Geyer, D. Martin, J. Tailleur, and D. Bartolo, Physical Review X **9**, 031043 (2019).
[8] M. N. Van Der Linden, L. C. Alexander, D. G. Aarts, and O. Dauchot, Physical Review Letters **123**, 098001 (2019).
[9] A. Cavagna, A. Cimarelli, I. Giardina, G. Parisi, R. Santagati, F. Stefanini, and M. Viale, Proceedings of the National Academy of Sciences **107**, 11865 (2010).
[10] A. Bricard, J.-B. Caussin, N. Desreumaux, O. Dauchot, and D. Bartolo, Nature **503**, 95 (2013).
[11] D. Geyer, A. Morin, and D. Bartolo, Nature materials **17**, 789 (2018).
[12] J. Deseigne, O. Dauchot, and H. Chaté, Physical Review Letters **105**, 098001 (2010).
[13] N. Kumar, H. Soni, S. Ramaswamy, and A. Sood, Nature communications **5**, 1 (2014).
[14] O. Chepizhko, E. G. Altmann, and F. Peruani, Physical Review Letters **110**, 238101 (2013).
[15] J. Toner, N. Guttenberg, and Y. Tu, Physical Review Letters **121**, 248002 (2018).
[16] J. Toner, N. Guttenberg, and Y. Tu, Physical Review E **98**, 062604 (2018).
[17] Y. B. Dor, E. Woillez, Y. Kafri, M. Kardar, and A. P. Solon, Physical Review E **100**, 052610 (2019).
[18] Y. Duan, B. Mahault, Y.-q. Ma, X.-q. Shi, and H. Chaté, Physical Review Letters **126**, 178001 (2021).
[19] B. Ventejou, H. Chaté, R. Montagne, and X.-q. Shi, Physical review letters **127**, 238001 (2021).
[20] S. Ro, Y. Kafri, M. Kardar, and J. Tailleur, Physical Review Letters **126**, 048003 (2021).
[21] Y. B. Dor, S. Ro, Y. Kafri, M. Kardar, and J. Tailleur, arXiv preprint arXiv:2108.13409 (2021).
[22] T. Vicsek, A. Czirók, E. Ben-Jacob, I. Cohen, and O. Shochet, Physical Review Letters **75**, 1226 (1995).
[23] A. P. Solon and J. Tailleur, Physical Review Letters **111**, 078101 (2013).
[24] J. Toner and Y. Tu, Physical Review Letters **75**, 4326 (1995).
[25] J. Toner and Y. Tu, Physical Review E **58**, 4828 (1998).
[26] J. Toner, Y. Tu, and S. Ramaswamy, Annals of Physics **318**, 170 (2005).
[27] J. Toner, Physical Review E **86**, 031918 (2012).
[28] B. Mahault, F. Ginelli, and H. Chaté, Physical Review Letters **123**, 218001 (2019).
[29] A. P. Solon, H. Chaté, and J. Tailleur, Physical Review Letters **114**, 068101 (2015).
[30] H. Chaté, F. Ginelli, G. Grégoire, and F. Raynaud, Physical Review E **77**, 046113 (2008).
[31] A. P. Solon and J. Tailleur, Physical Review E **92**, 042119 (2015).
[32] J. V. José, L. P. Kadanoff, S. Kirkpatrick, and D. R.

Nelson, Physical Review B **16**, 1217 (1977).
[33] S. Elitzur, R. Pearson, and J. Shigemitsu, Physical Review D **19**, 3698 (1979).
[34] J. Tobochnik, Physical Review B **26**, 6201 (1982).
[35] C. M. Lapilli, P. Pfeifer, and C. Wexler, Physical Review Letters **96**, 140603 (2006).
[36] Z.-Q. Li, L.-P. Yang, Z.-Y. Xie, H.-H. Tu, H.-J. Liao, and T. Xiang, Physical Review E **101**, 060105 (2020).
[37] These rates are chosen such that, for isolated sites, the dynamics would satisfy detailed balance with steady-state probabilities $P_{\mathbf{R}} = \exp[-\beta H_{\mathbf{R}}]$ and $H_{\mathbf{R}} = -m_{\mathbf{R}}^2/(2\rho_{\mathbf{R}})$.
[38] See supplementary information online.
[39] For the AIM, the same phenomenology is found for any activity $\varepsilon > 0$ [31]. We have no reason to suspect a different behavior in our active clock model.
[40] While this fit cannot be perfect, since the structure factor of the isotropic model is expected [24–27] to scale like $k^{-\nu_{\parallel,\perp}}$ with neither $\nu_{\parallel}$ nor $\nu_{\perp}$ equal to 2, both exponents are close enough to 2 that this fit suffices to give a good estimate of ξ_q.
[41] A. Solon, H. Chaté, J. Tailleur, and J. Toner, In preparation.
[42] We measure σ in the active XY model (*i.e.* with $q = \infty$) by fitting the distribution $P(\theta_{\mathbf{R}} - \langle\theta\rangle)$ with $\theta_{\mathbf{R}}$ the local orientation on site $\mathbf{R}$ to a normal distribution. We find $\sigma^2 \approx 0.22$ for the parameters of Fig. 2c.